Modelling and Validation of Microstructure Replication on Aluminum Foils from Laser-Patterned Stamps

Stephan Moghtaderifard*[1], Marcos Soldera[1], and Andrés Fabián Lasagni[1,2]

[1]*Institut für Fertigungstechnik, Technische Universität Dresden, George-Bähr-Str. 3c, 01069 Dresden, Germany*
[2]*Fraunhofer-Institut für Werkstoff- und Strahltechnik IWS, Winterbergstr. 28, 01277 Dresden, Germany*
**Corresponding author's e-mail:* stephan.moghtaderifard@tu-dresden.de

Aluminum foils are commonly used in food and pharmaceutical packaging due to their outstanding combination of malleability, low cost, oxygen barrier and light reflectivity. Extra functionalities, like hydrophobicity or structural coloration, can be added to them by engineering topographical surfaces microstructures. In this work, cold embossing method is used to replicate microstructures from pre-structured stamps onto aluminum foils. The Direct Laser Interference Patterning (DLIP) method is used to structure periodic line-like textures on stainless steel plates. The produced stamps are employed to imprint the Al foils under different controlled pressures. A good transfer of the microtextures to the Al based material was observed, with a 6-40% relative difference in the structure depths between master and replica depending on pressure and aspect ratio of the structures on the steel mold. Although a complete replication of the stamp textures is not obtained due to incomplete stamp cavities filling and elastic recovery, the achieved structural coloring demonstrates a uniform microtexture on the foils. A model based on the finite element method is developed and validated by comparing the simulation results with the microstructured aluminum foils, yielding relative differences in the simulated and experimental structures depths below 20%.
DOI: 10.2961/jlmn.2022.02.2004
Keywords: direct laser interference patterning, cold embossing, replication, surface microstructures, Finite Element Method, structural mechanics

1. Introduction

Aluminum (and aluminum alloys) has become an essential material in many applications due to its unique combination of properties, such as high strength to weight ratio, excellent thermal and electrical conductivity and high resistance to corrosion. Particularly, aluminum thin foils are widely used for packaging applications because this material is effective as a barrier against gases and moisture. Furthermore, its manufacturing costs are relatively low and it can be easily recycled [1, 2].

Additional functionalities, like hydrophobicity or structural coloration, can be added to Al foils by engineering surface microstructures. Several micropatterning techniques have been applied on thin metal foils, such as electromagnetic forming, laser shock forming, laser embossing, direct laser writing and plasma printing. However, these methods are relatively complex, involve multiple processing steps including coatings deposition, and high-throughputs have not been demonstrated. All this limits their applicability for industrial manufacturing [3-7]. Replication methods based on conventional manufacturing processes, such as cold embossing, can achieve high throughputs using a single pre-patterned stamp [8]. There are many different fields where embossing is used, for example, in the micromechanical, microoptical [9], chemical, medical and biological fields [10]. The microstructures of the embossing tool can be created by various manufacturing processes like micromilling, Diamond Micro Chiseling (DMC) or photolithography [11-14]. If high flexibility is also required, for example for engraving decorative logos with complex geometries, one-step laser-based methods are well-suited for both rapid-prototyping and mass production [15]. Several laser-based methods have been employed to create the structures on stamps (or molds) [16, 17]. However, to keep the processing costs low, especially for packaging applications, new high-throughput and low-cost microprocessing technologies are required. A cost-effective process for surface texturing is Direct Laser Interference Patterning (DLIP) method [18]. DLIP is able to fabricate periodic textures on the surface of various materials such as metals, ceramics or polymers with a high degree of flexibility and resolution down to the sub-micron range using pulsed lasers with pulse durations in the fs to ns range [15, 19, 20]. This method can be scalable to high-throughputs and large-areas compatible with industrial requirements [21]. This method relies on the overlap of two or more laser beams on the sample surface to originate an interference pattern [22, 23]. At the maxima positions, the material can be locally melted or ablated producing a repetitive surface microtexture. The resulting proportion of molten or ablated material depends on the interaction between the laser radiation and the material. One of the most important factors governing the material removal and microstructure formation is the laser pulse duration. Using pulse durations in

the ns scale is an effective and relatively low-cost approach to fabricate microstructured surfaces by DLIP [24]. However, the strong thermal effects and the large amount of molten material and debris distributed on the surfaces when irradiating with a ns-laser source can pose significant challenges concerning the topography homogeneity as well as undesired chemical or structural modifications [25]. These disadvantages inherent of the ns-lasers can be avoided upon employing ultra-short pulsed (ps to fs regime) lasers which allow smaller structures with better regularity due to minimal thermal effects [26]. In this way, different surface functionalities can be reached without the utilization of chemicals or coatings. Therefore, as many laser-based treatments, DLIP can be considered to be environmentally friendly [27-31].

Al materials have been already treated using DLIP technique with ps and ns pulses [32-35]. In this frame, periodic structures with line and dot-like geometries were produced, having spatial periods ranging from 2.6 µm to 19.0 µm. However, to our best knowledge, Al foils have not been so far textured using metallic stamps processed with DLIP.

In this study, laser-microtextured stamps are produced using DLIP and utilized for the embossing of Al-foils at atmospheric conditions. A numerical model using Finite Element Methods (FEM) is presented for the cold embossing process in order to understand and optimize the process, [36, 37]. In this way, limitations of the achievable microstructures relative to the stamp geometry are discussed. The fabricated textured surfaces are characterized using optical confocal microscopy and scanning electron microscopy (SEM) techniques.

2. Materials and methods

2.1 Materials

An austenitic stainless steel plate with the material specification 1.4301 (X5CrNi18-10) was patterned by DLIP and used as stamp. The substrate had a thickness of 0.8 mm with an average surface roughness (R_a) of 52 nm ± 10 nm and a surface area of 50 cm^2. After laser processing, the samples were stored under atmospheric conditions.

For the cold embossing tests, aluminum foils (EN AW-1050) from ALUXFOIL BÁZIS Ltd. Were used, with thickness of 50 µm. The purity of the Al foils was 99.5%. The microstructures from the laser-patterned stamps were transferred to the shiny side of the foil characterized by an average arithmetic height S_a of 175 nm and a RMS height S_q of 229 nm. The foils were used as received.

2.2 Direct laser interference patterning setup

DLIP was used to fabricate the patterned stamps for embossing. An in-house developed DLIP system (TU Dresden/Fraunhofer IWS, Germany) with an optical head based on 10 ps laser source (Edgewave PX200, Germany) operating at a 1064 nm wavelength was employed to engrave periodic line-like textures on a stainless steel plate, The laser had a nominal maximum output power of 10 W and the repetition rate was set to 1 kHz. The setup and schematic beam flow in the optical head as well as a representation of the resulting line-like structure are shown in Fig. 1.

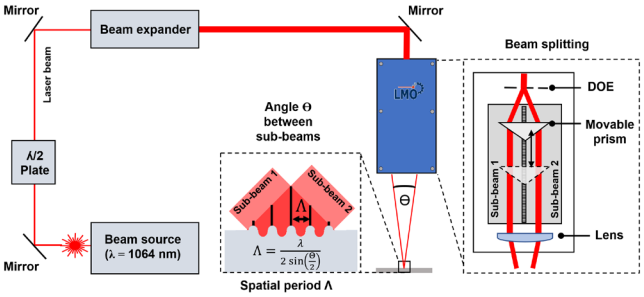

Fig. 1 Schematic representation of the two-beam direct laser interference patterning setup. In the DLIP module, the primary beam is split into two sub-beams by the DOE, which are overlapped at the sample surface by a convex lens. The resulting spatial period Λ is given by the equation in the inset.

The laser beam power was controlled with a half-wave plate and the spot size at the sample was adjusted with a beam expander (see Fig. 1). The primary beam was guided to a diffractive optical element (DOE) which split the laser beam into two sub-beams with the same intensity. Then, the sub-beams were parallelized by a prism, which can be translated so that the interference angle θ can be adjusted, ultimately allowing the user to fine-tune the spatial period Λ of the patterned texture (see Fig. 1). With the help of a convex lens, the sub-beams were overlapped on the sample surface [38-40]. In this work, the spatial period was fixed to 4.9 µm for all samples. Fully structured areas were fabricated by overlapping single laser pulses in the direction parallel and perpendicular to the DLIP interference lines. The pulse-to-pulse overlap (OV) is given as the percentage of superposition of adjacent pulses in the direction parallel to the DLIP lines and it was varied from 85 % to 95 %. The hatch distance (HD) represents the distance between the pulses in the direction perpendicular to the interference lines and it must be a multiple of the spatial period to avoid destroying the repetitive textures during the sequential patterning. Considering that the spatial period was 4.9 µm the HD was varied from 24 µm to 34 µm. Employing the D2 method [41], a threshold fluence of 0.55 J/cm² was obtained for the stainless steel and a spot diameter of 115 µm was calculated.

2.3 Embossing procedure

A four-column electro-hydraulic press (HKP 400, P/O/WEBER, Germany) was used for embossing the structures on aluminum foil from the DLIP-patterned stamp. The force evolution consisted of three steps. In the first step, the force was ramped for 60 s until it reached the holding force. Then, the force was kept constant for 120 s and finally it was slowly released during another 60 s. The stamp was pressed onto Al foils at three different force levels of 150, 300 and 600 kN which correspond to 37, 72 and 145 MPa, respectively. The process was carried out at room temperature. Two 1 mm-thick soft rubber sheets were placed on top of a steel counter plate and below the stamp to provide a uniform pressure distribution over the surface.

2.4 Topography characterization

The topography of the fabricated textures on both steel and Al was measured by a non-contact optical confocal microscope (CFM, Sensofar S Neox 3D Surface Profiler,

Spain) equipped with a 150X objective. The evaluation of the topographic data was performed by the software SensoMAP Premium and the geometrical parameters, like shape, period, and aspect ratio were determined. The samples were also characterized using a scanning electron microscope (SEM) at an operating voltage of 30 kV (Quattro ESEM, Thermo Fischer Scientific, Germany).

2.5 Finite Element Method simulation

A model based on the finite element method and implemented in COMSOL® Multiphysics© (version 5.6) was developed to simulate the embossing process. The FEM model was solved using the Structural Mechanics module and Time Dependent study. The Newton-Raphson (N-R) algorithm was used to solve the equations describing the elastic-plastic behavior of the Al material in the simulations.

3. Results and discussion

3.1 DLIP structuring of stamps

On the stainless steel plate, a matrix with 9 fields was patterned with different hatch distances and pulse overlaps. Each field had an area of 15 × 15 mm^2. A fixed spatial period of 4.9 µm was used in all fields. The chosen hatch distance was 5, 6 and 7 times the spatial period corresponding to 24.5, 29.4 and 34.3 µm, respectively, whereas the selected overlap values were 85%, 90% and 95%. The fluence per pulse was kept constant at 2.2 J/cm².

The average structure depths of the patterned fields on the stamp are shown in Fig. 2. It can be observed that the structure depth depended strongly on HD and OV. With the same pulse energy, deeper structures could be achieved by increasing the pulse-to-pulse overlap in the direction parallel to the line-like pattern [32]. Likewise, as the hatch distance decreased, the cumulated deposited energy per area (or cumulated fluence) increased, yielding deeper grooves. A maximum aspect ratio (depth-to-period ratio) of 0.31 was achieved for the field structured with OV = 95% and HD = 34.3 µm.

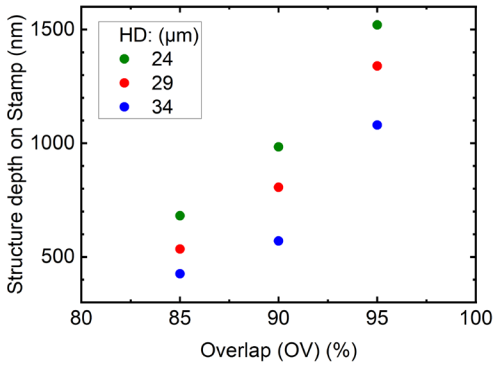

Fig. 2 Effect of pulse overlap and hatch distance on structure depth.

Fig. 3 shows confocal (a) and SEM (b) images of a selected DLIP-structured field. Namely, the surface was structured at OV = 95% and HD = 24.5 µm. Also a profile extracted from the confocal measurement is shown. A uniform arrangement of parallel grooves can be noticed in both images. In the case of the SEM image, a sub-structure consisting of quasi-periodic ripples with 600-700 nm period is observed (see inset in Fig. 3b), which can be identified as Laser Induced Periodic Surfaces Structures (LIPSS). As these ripples were aligned perpendicular to the polarization of the laser and their size is larger than half of the laser wavelength, they can be identified as Low-Spatial Frequency LIPSS (LSFL) [42].

Considering that iron is the primary constituent of stainless steel, the thermal diffusion length l_T can be calculated as $l_T = (\kappa\, \tau_P/\rho\, c_p)^{1/2}$ assuming a thermal conductivity $\kappa = 80.2$ W/m K, a heat capacity $c_p = 449$ J/kg K and a density $\rho = 7.87$ g/cm^3 [43]. As the laser source emitted pulses with a pulse duration $\tau_P = 10$ ps, a heat diffusion length of only 15 nm can be assumed for stainless steel. This strongly suggests that the heat-affected zone (HAZ) induced at the maxima positions of the interference pattern is very localized and does not interact with the adjacent HAZ around the other maxima positions. As a consequence, it can be assumed that cold ablation with probably only little melting took place at the maxima positions, whereas at the minima positions the material remained unaffected. As can be observed in the SEM image, practically no molten material or debris can be visualized, supporting this statement. Nevertheless, the LIPSS were visible also around the minima positions, implying a material modification and rearrangement. Although around the minima positions the local laser fluence was relatively small, a pulse-to-pulse overlap of 95% was used to fabricate such stamp, implying 20 pulses per spot, and thus significant cumulated fluence allowing the formation of such LIPSS.

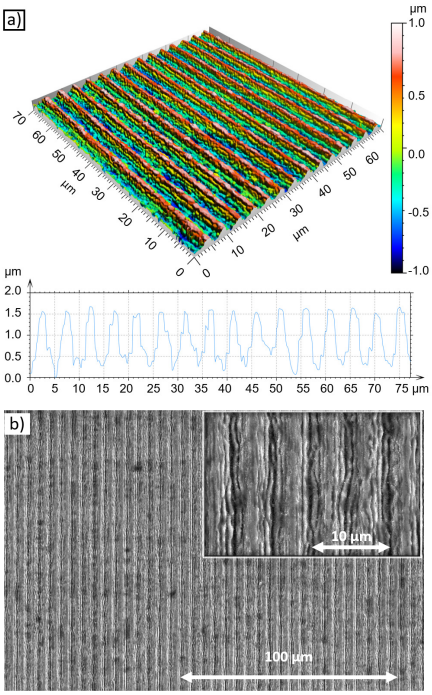

Fig. 3 a) Confocal and b) SEM images of a selected DLIP-structured field with h = 1.5 µm, OV = 95% and HD = 24.5 µm.

3.2 Replication of the microstructures on Al foils

In all cold embossing experiments, the stamp was pressed onto the Al foils so that the microstructures could be replicated. The Al foil was placed between the structured stamp and an untreated steel plate as counterpart. To prevent the stamp from sticking to the electro-hydraulic press, two 1 mm thick soft rubber foils were placed be-

tween the counterpart and upper press plate and between the backside of the stamp and lower press plate. In addition, this soft foil favored a uniform pressure distribution on the stamp [44]. The temperature was kept at 25°C constant for all experiments. The evolution of the applied pressure was implemented in three steps. In the first step, the pressure was ramped with a linear slope to a defined holding value for 60 seconds. In the second phase, the pressure was kept constant for 120 seconds and finally, the force was released with the same slope as the first step for another 60 seconds.

The microstructures from the steel stamps were transferred to Al foils by cold embossing applying three different holding pressures, namely 37, 72 and 145 MPa. Fig. 4 shows photographs of the a) DLIP textured steel plate and the embossed foils using a load of b) 145 MPa, c) 72 MPa and d) 37 MPa. Due to the successful and uniform replication of the repetitive microstructures of the stamp, all embossed foils show the characteristic holographic coloration arising from surface relief diffraction gratings.

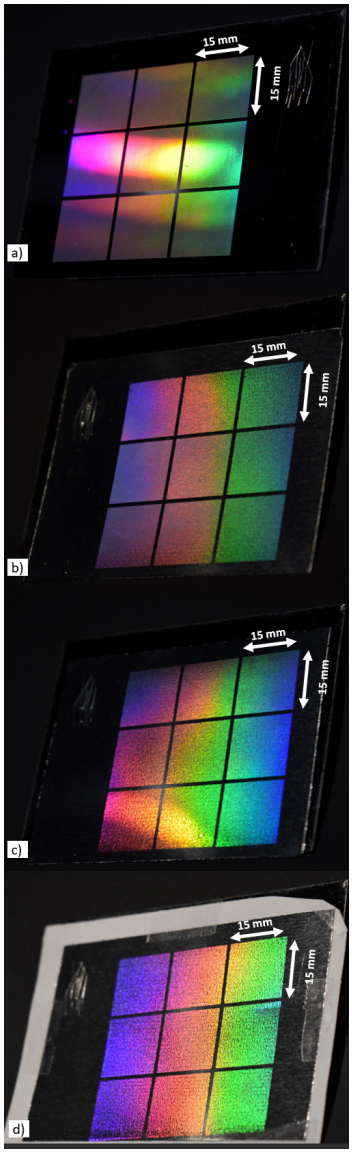

Fig. 4 Photographs of DLIP treated stamp (a) and embossed aluminum foils showing the structural coloration applying a load of b) 145 MPa c) 72 MPa and d 37 MPa.

The confocal and SEM images in Fig. 5 were taken on imprinted Al foils from the stamp treated with OV = 95% and HD = 24.5 µm at a pressure of 145 MPa (Fig. 5 a,b) and 72 MPa (Fig. 5 c,d). Although, in both cases the periodic line-like textures could be successfully reproduced, the imprinted foil at a pressure of 145 MPa had 16% deeper structures than the ones embossed at 72 MPa (see profiles extracted from the confocal measurements in Fig. 5).

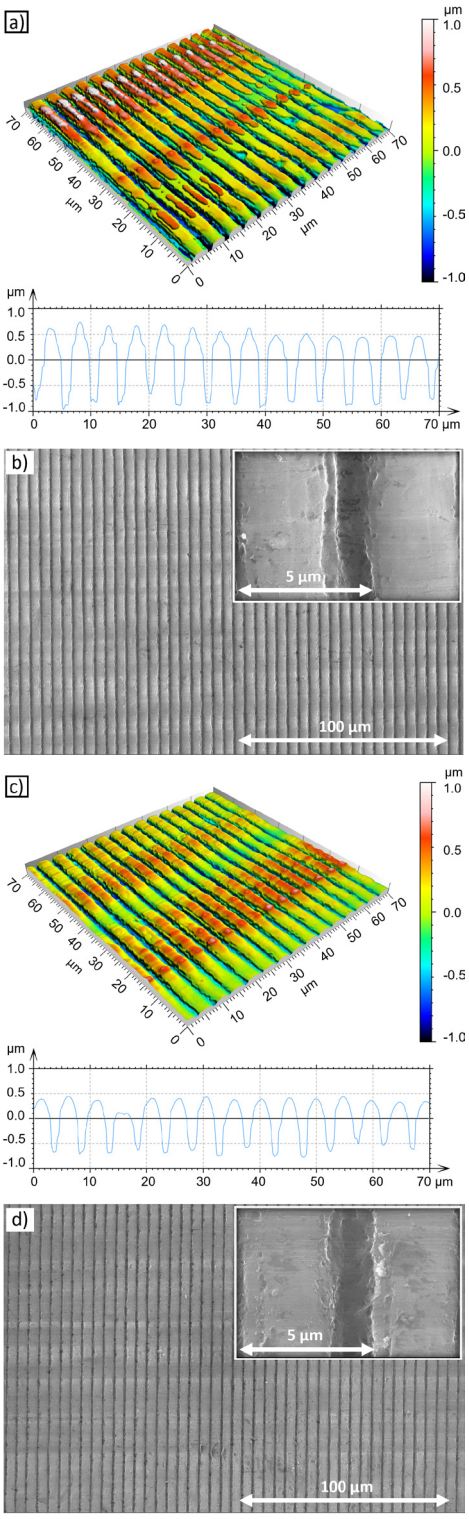

Fig. 5 Confocal images of embossed aluminum foils under the load of a) 145 MPa c) 72 MPa and b,d) corresponding SEM images.

Based on the SEM images and the extracted profiles, it can be noticed that the grooves on the Al foil produced at

145 MPa are not only wider than the foil imprinted at 72 MPa, but also that the LIPSS features were transferred on the edges of the embossed grooves when the highest pressure was applied. On the contrary, the LIPSS present on the valleys of the stamps were not fully transferred to the Al foil. Moreover, the ridges on the Al foil have a relatively smooth appearance (see for example the inset of Fig. 5d). This can be ascribed to an incomplete filling of the stamp cavities by the Al material, due to its rigidity. As a consequence, the LSFL decorating the DLIP line-like texture were not fully transferred to the Al.

Fig. 6 summarizes the measured structure depth on the Al foils as function of the depth of the corresponding stamp. It can be observed that as the applied pressure increased, the textures on the Al foils are deeper and the difference between the depths of the stamp and imprint decreased. The average depth differences between the Al-foil and the stamp were 47% at a load of 37 MPa, 35% at 72 MPa and 17% at 145 MPa.

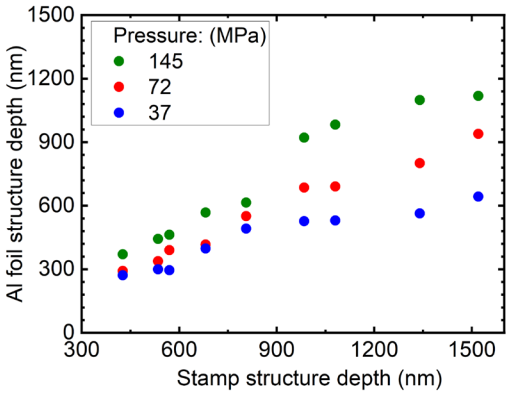

Fig. 6 Experimental structure depth of microtextures on the Al foil under the application of different load levels.

3.3 FEM simulation of the embossing process

For setting the simulation domain, it is considered that the cross section of the stamps is constant in the Z-direction. Therefore, a 2D simulation domain lying in the XY plane was used, assuming that the grooves of the stamp have an infinite length in Z-direction, as shown in Fig. 7. In addition, it is considered that the microstructures are homogeneous and symmetrical, and thus a 2D model of a half of single groove was simulated (Fig. 7b). Similar considerations were employed in the work of Narijauskaitė et al, but for simulating a hot imprint process of polycarbonate [45]. Furthermore, it is considered that the lateral boundary conditions are periodic and the local displacement on them is zero. In this way, the calculation cost can be strongly reduced by solving the problem within a repetitive unit of the periodic assembly.

Regarding the domain geometries, two conditions were assumed for ensuring realistic results with a satisfactory convergence. Firstly, the geometry of the stamp microstructures was modeled by using the envelope of three overlapped circles, whereby their radius and positions were fitted for each stamp field according to the profiles extracted from confocal measurements. The second assumption is that the initial distance between the aluminum foil and the stamp is zero, as shown in Fig. 7. This consideration enables a better build-up of the contact problem between the two bodies (stamp and foil) and to a better convergence.

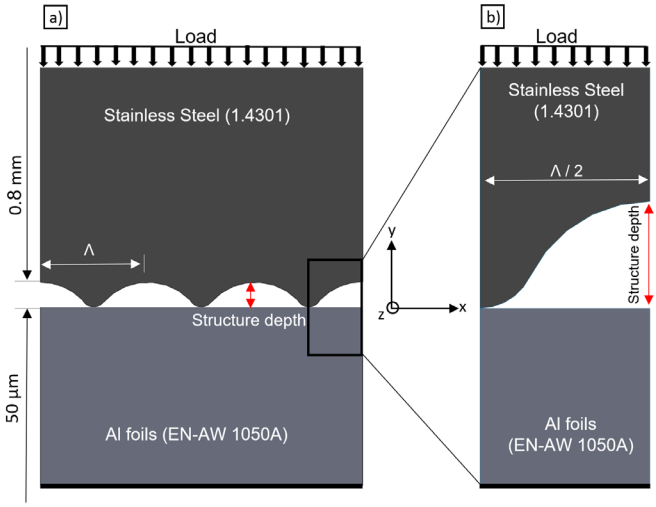

Fig. 7 a) General representation of the model, b) used geometry for the FEM model.

Two materials were used in the model, namely stainless steel for the stamp and aluminum for the foils. The adopted material properties are described in Table 1, which were provided by the manufacturers or taken from the literature [46, 47]. It is considered that both materials can enter the elastic-plastic regime when they come into contact.

Table 1 Material properties of aluminum foil and stainless steel [46, 47].

Property	Stainless Steel 1.4301	Aluminum EN AW-1050
Young's modulus [GPa]	200	70
Density [g/cm^3]	7.9	2.7
Poisson's ratio [-]	0.28	0.33

Due to the high Young's modulus of steel, this material did not undergo plastic deformation for the range of pressures used in the present simulations. In the case of the Al foils, it was assumed an isotropic hardening regime and that the plasticity behavior can be described by Voce equation. The corresponding parameters were taken from the work of Käck et al. [48] as well as COMSOL's database and the Al foil supplier. Namely, a yield strength of 35 MPa, a saturation stress of 35 MPa and an exponential hardening of 26 were used in the model implemented in COMSOL.

Next, the effect of the size of the triangular mesh on the aluminum forming was studied by running simulations with varying minimum element size from 0.2 µm to 2.4 µm and by using three loads (37, 72, 145 MPa). Generally, the maximum deformation of the Al and the maximum stress on the Al foil did not depend strongly on the mesh size (not shown). However, the resulting shape of the replicated microstructures had a significant dependence on the used mesh size, as finer meshes can map with higher resolution the cavities of the stamp. In addition, taking into account the mesh-dependent calculation time, all simulations were performed with a mesh size of 0.4 µm and 0.2 µm for the

stamp and the foils, respectively, resulting in less than 2000 elements for all simulated geometries. On average, all simulation runs took less than 60 s to be solved.

The pressure was applied following a time-dependent function with a triangular shape so that the pressure was increased linearly until it reached the set pressure and then it was released linearly until detachment of both materials. As viscoelastic or viscoplastic effects on Al were disregarded in the simulations, the time scale for ramping or releasing the pressure was not relevant.

Intermediate steps of a typical simulation run are displayed in Fig. 8, which illustrates the forming process of aluminum. Fig. 8a describes the initial Al and steel domains of the model without applied load. In Fig. 8b, a relatively low load is applied and the foil enters into the elastic regime. In this regime, if the force is removed, the Al resumes its original shape. When the load is further increased, the plastic deformation phase is reached (Fig. 8c) and thus the deformation is then considered to be permanent. It was noticed that a complete filling of the stamp cavities was not achieved for the simulated geometries and pressures, which ultimately prevents a faithful replication of the microtextures on the foils. Finally, Fig. 8d shows the calculation results after the unloading phase, where a part of the deformation (elastic range) vanished. As expected, only the aluminum material was deformed and the stainless steel stamp remained unchanged.

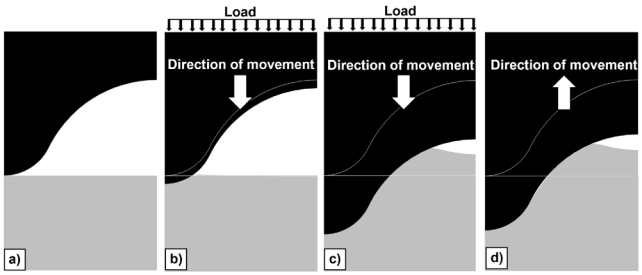

Fig. 8 The principle of model behavior at a) initial stage, b) elastic regime, c) plastic regime, and d) unloading stage.

Fig. 9 shows the influence of the applied pressure on the resulting structure depth on the Al foils imprinted with stamps with different depths, i.e., 426, 681 and 1520 nm. As the pressure was increased, the structure depth increased linearly up to a point where it saturated to a value relatively close to the depth of the corresponding stamp. In all cases, the depths in the Al material did not reach those of the stamps because of the reversible deformation in the elastic regime and due to the incomplete filling of the stamp cavities (as discussed before, see Fig. 8d). The plot also shows that the deeper the structures on the stamps, then the higher the applied force must be to reach the saturation depths on the foils. The simulations also suggest that for reaching the maximum deformation using a stamp with a depth of 1520 nm, a pressure of approximately 300 MPa must be applied, whereas for replicating a structure depth of 426 nm, a pressure of ~160 MPa is sufficient.

Fig. 10 shows the simulated depths on the Al as function of the depth on the corresponding stamp structures. It was observed that the depth of the Al microtextures increased approximately linearly with the stamp depth for applied pressures of 72 and 145 MPa. However, for 37 MPa the depth on the Al tended to saturate around a value of 150-180 nm. The relative difference of the depths in stamps and replica ranged from 67% to 88% for 37 MPa, while this difference was between 37% and 40% for 72 MPa and between 6% and 14% for 145 MPa.

It became evident that the foil could not be successfully deformed at a load of 37 MPa, probably due to the fact the assumed yield strength of aluminum of 35 MPa was slightly lower than the assumed pressure. Therefore, this load was not enough to induce a large deformation in the foil.

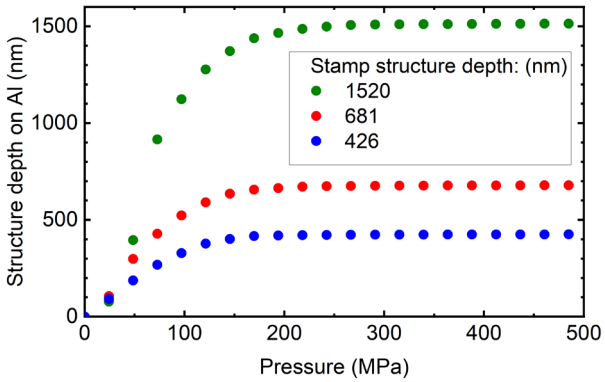

Fig. 9 Simulated structure depth of the periodic elements at the Al foils depending on the applied load.

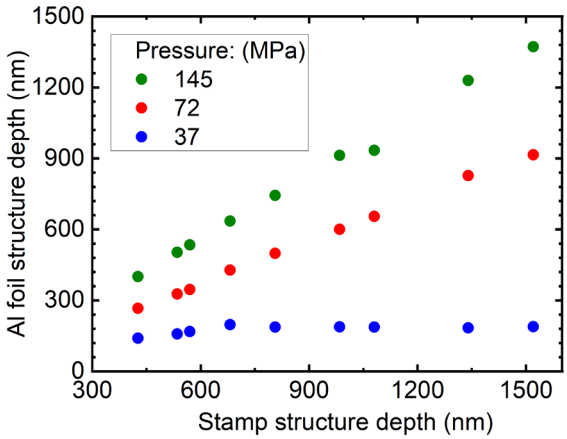

Fig. 10 Simulated structure depth of Al foil as function of the depth of the employed stamp for the different applied pressures.

Fig. 11 shows the stress distribution in the aluminum foil using different load levels and stamp structure depths. The resulting stress was calculated according to the von Mises criterion. All replicas that are in the same row were obtained from the same stamp structure depth (see labels on the left-hand side of Fig. 11), whereas the columns represent different applied load (see labels in the top-part of the image). It was found that for all feature sizes of the stamp, as the pressure increased from 37 MPa to 145 MPa, the deformation in the Y-direction increased and the areas with high stress (red) increased significantly, especially under the stamp protrusion. Likewise, an increase in the stamp depth led to higher deformations and stresses. It can be noted that the Al material raised above the initial surface (gray line), due to the plastic deformation from the area below the stamp protrusion towards the stamp cavities (from left to right in the images of Fig. 11).

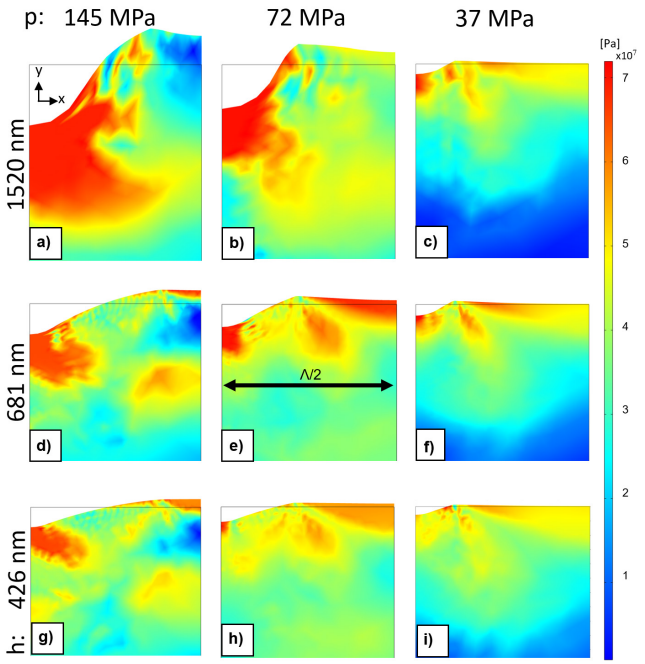

Fig. 11 Final stress distribution and deformation of the Al foil as a function of the applied pressure for the stamp structure depth of 1520 nm (a, b, c), 681 nm (d, e, f) and 426 nm (d, h, i) using a load of 145 MPa (a, d, g), 72 MPa (b, e, h) and 37 MPa (c, d, i).

To study the processability of Al by cold embossing for different spatial periods of stamp structures, the structure depth on the Al foils as function of the applied pressure for four selected periods is plotted in Fig. 12. In all simulations, the aspect ratio was kept constant at 0.3. It is visible that the structures on Al with a spatial period larger than 1.3 µm reach the saturation regime at approximately the same pressure, i.e. 200 MPa. However, for the smallest analyzed period (0.8 µm), the saturation regime can only be approached at extremely large pressures of more than 600 MPa, which limits the applicability of this approach for textures with sub-micro textures.

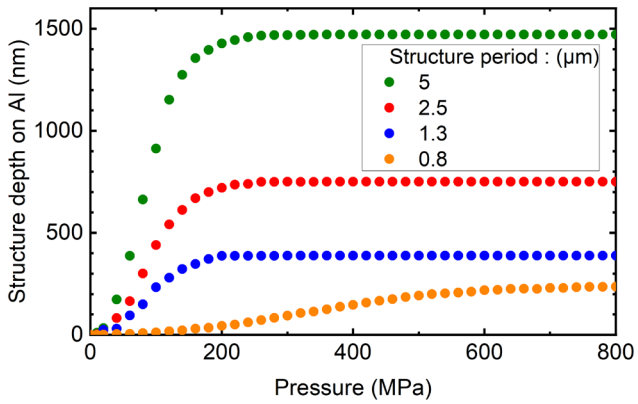

Fig. 12 Simulated structure depth of Al foil as function of the applied pressure and spatial period of stamp texture.

3.4 Validation of the model

For validating the model, the simulation results were compared with the experiments assuming equivalent stamp geometries and applied loads. In Fig. 13 the simulated structure depths on Al foils after the embossing process (y-axis) are plotted against the experimental results (x-axis) with the corresponding stamp characteristics. Namely, each datapoint corresponds to the same stamp geometry in both simulation and experiment.

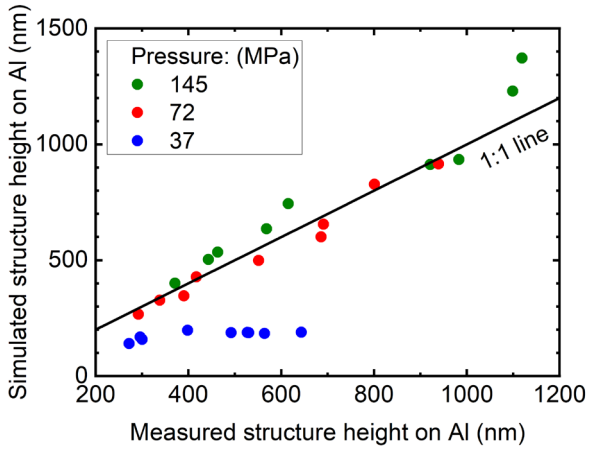

Fig. 13 Validation of the FEM model through a comparison between the simulated and experimental structure depths on the Al foils at different pressures.

The black line stands for a linear relation with a slope equal to unity, so that datapoints lying on top of the line represent a perfect match between simulation and experiment. It can be seen that for applied pressures between 72 and 145 MPa, a very good agreement between both the simulated and experimental results was found for the whole explored range of depths, i.e. from 300 nm to 1100 nm. The average relative error was 8.9% in this range. The maximum deviation of the simulations compared to the experiments corresponded to the deepest structures, i.e. 1120 nm. In this case, the simulated depth was 18% higher than the experiments.

In the case of the runs simulated for a pressure of 37 MPa, the simulated depths were significantly lower than the experimental values, and a maximum deviation of 70% was observed. This behavior can be attributed to the fact that the assumed yield strength of 35 MPa for Al, was slightly lower than the applied pressure of 37 MPa, preventing a large deformation of the foil. Further studies are needed to characterize the mechanical properties of the used Al foil in order to refine the value of the parameters that describe its behavior in the plastic regime.

4. Conclusions

In this study, periodic textures were produced on stainless steel by Direct Laser Interference Patterning (DLIP) employing a ps-pulsed laser source. Uniform line-like microstructures were fabricated with a spatial period of 4.9 µm and structure depths ranging from 300 nm to 1520 nm. The steel plate was used as a stamp in a cold embossing process to transfer the microtextures onto commercial aluminum foils. The topographical characterization of the treated foils revealed a satisfactory replication of the stamp features. Moreover, at high pressures (145 MPa) even nanoripples (LIPSS) with a spatial period in the range 600 nm – 700 nm, were transferred within the cavities of the micropatterned foils. Furthermore, differences between

the structure depths on stamp and replica were as low as 6%.

A simulation model based on the finite element method was developed to understand the embossing process as well as to predict the achievable structure shapes and depths on the replicated textures. The model was validated by comparing the simulation results with the experimental values of the feature depths of the Al foils depending on the applied load and the depth of the structures of the stamp. For pressures of 72 and 145 MPa, the relative error varied between 1 and 20% (mean value ~ 9%). In case of the lower pressures (37 MPa), the measured depth in the experiments were larger compared to the simulations, probably due to an overestimated Al yield strength in the model. The simulation results have also shown that the microstructures could be successfully transferred to Al foil for spatial periods at least larger than 1.3 µm (with an aspect ratio of 0.3). Further experimental studies should be conducted to validate this statement.

The proposed approach to functionalize Al foils by replicating a microtexture from a DLIP-treated stamp can represent an important step in the development of low-cost surface texturization of multifunctional packaging, with enhanced anti-bacterial or decoration properties.

Acknowledgments

The work of A.F.L. is also supported by the German Research Foundation (DFG) under the Excellence Initiative program by the German federal and state government to promote top-level research at German universities.

References

[1] A. Emblem and H. Emblem: "Packaging technology: Fundamentals, materials and processes" (Woodhead Publishing Limited, Sawston, 2012) p.163.
[2] R. Ranau, J. Oehlenschläger, and H. Steinhart: Food Chem., 73, (2001) 1.
[3] T. Shiratori , T. Aizawa , Y. Saito , K. Dohda: Materials, 12, (2019) 2640.
[4] D. Huang, J. Man: Coatings, 10, (2020) 1264.
[5] J. Man, J. Zhao, H.Yang, L. Song, D. Liu: Mater. Des., 193, (2020) 108822.
[6] Q. Zhao, C.Wang, J. Xu, D. Shan, B. Guo: Manufacturing Rev.: 2, (2018) 7.
[7] R. Jagdheesh, J.J. García-Ballesteros, J.L. Ocaña: Appl. Surf. Sci., 374, (2016) 2.
[8] J. Böhm, A. Schubert, T. Otto, and T. Burkhardt: Microsyst. Technol., 7, (2001) 191.
[9] H. Ottevaere ,S. van Overmeire, J. A. Silvestre, L. Nieradko, G Desmet, C. Gorecki, H. Thienpont:
[10] H. Mekaru, T. Yamada, S. En, and T. Hattori: Proc. MNC 2002, (2002) 192.
[11] S. Tsai, P. Chen, S. Huang, Y. Lee: Microelectron. Eng., 150, (2016) 19.
[12] L. Langstädtler, L. Schönemann, C. Schenck, B. Kuhfuss: J. Micro Nano-Manuf., 4, (2016) 2.
[13] H-D. Yu, X-R. Zhang, Y-L. Wan, J-k. Xu, Z-J. Yu & Y-Q. Li: Surf. Eng., 32, (2016) 108.
[14] X. Zhang, Y. Wan, B. Ren, H. Wang, M. Yu, A. Liu, Z. Liu: Micromachines, 11, (2020) 316.
[15] E. I. Ageev, V. P. Veiko, E. A. Vlasova, Y. Y. Karlagina, A. Krivonosov, M. K. Moskvin, G. V. Odintsova, V. E. Pshenichnov, V. V. Romanov, and R. M. Yatsuk: Opt. Express, 26 (2018) 2117.
[16] H . Y. Erbil, A. L. Demirel, Y. Avci, and O. Mert: science, 299, (2003) 1377.
[17] A. Kovalchenko, O. Ajayi, A. Erdemir, G. Fenske, and I. Etsion: J. Tribol. Int., 38, (2005) 219.
[18] A. F. Lasagni: Adv. Opt. Technol., 6, (2017) 265.
[19] L. Müller-Meskamp, Y. Kim, T. Roch, S. Hofmann, R. Scholz,S. Eckardt, K. Leo, A. F. Lasagni: Adv. Mater., 24, (2012) 906.
[20] M. Bieda, E. Beyer, A. F. Lasagni: J. Eng. Mater. Technol., 132, (2010) 031015.
[21] F. Ränke, R. Baumann, B. Voisiat, A. F. Lasagni: Mater. Lett.,14, (2022) 100144.
[22] A. F. Lasagni, T. Roch, J. Berger, T. Kunze, V. Lang, E. Beyer: Proc. SPIE 2015, (2015) 9351.
[23] P.Graus, T. B. Möller, P. Leiderer, J. Boneberg, N. I. Polushkin: Opto-Electron Adv, 3, (2020) 190027.
[24] V. Furlan, M. Biondi, AG. Demir, G. Pariani, B. Previtali, A. Bianco: Appl. Surf. Sci., 423, (2017) 619.
[25] Z. Lin, M. Hong: Ultrafast Sci., 2021, (2021) 9783514.
[26] F. Fraggelakis, GD. Tsibidis, E. Stratakis: Opto-Electron. Adv., 5, (2022) 210052.
[27] M. D'Alessandria and F. Mücklich: Appl. Phys. A, 98, (2009) 311.
[28] A. Rosenkranz, M. Hans, C. Gachot, A. Thome, S. Bonk, and F. Mücklich: Lubricants, 4, (2016) 2.
[29] F. Rößler, T. Kunze, and A. F. Lasagni: Opt. Express, 25, (2017) 22959.
[30] T. Kunze and A. F. Lasagni: Proc. Lasers in Manufacturing Conference, (2017) 1.
[31] T. Jähnig, A. Mousavi, V. Lang, T. Kunze, A. Brosius, and A. Lasagni: Dry metal forming, 4, (2018) 62.
[32] J.T. Cardoso, A.I. Aguilar-Morales, S. Alamri, D. Huerta-Murillo, F. Cordovilla, A.F. Lasagni, J.L. Ocaña: Opt. Lasers Eng., 111, (2018) 193.
[33] S. Milles, B. Voisiat, M. Nitschke, and A. Lasagni: J. Mater. Process. Technol., 270, (2019) 142.
[34] V. Lang, B. Voisiat, and A. Lasagni: Materials, 12 (2019) 1484.
[35] S. Milles, M. Soldera, T. Kuntze, and A. F. Lasagni: Appl. Surf. Sci., 525, (2020) 146518.
[36] G. Cheng, M. Sahli, J. C. Gelin, and T. Barriere: J. Mater. Process. Technol., 229, (2016) 36.
[37] G. Cheng, J. C. Gelin, and T. Barriere: Proc. CFM 2011, (2011) 03422661.
[38] M. Soldera, F. Fortuna, S. Teutoburg-Weiss, S. Milles, K. Taretto, and A. Lasagni: J. Laser Micro Nanoeng., 15, (2020) 97.
[39] M. Soldera, Q. Wang, F. Soldera, V. Lang, A. Abate, and A. F. Lasagni: Adv. Eng. Mater., 22, (2020) 1901217.
[40] A. Lasagni, T. Roch, M. Bieda, D. Benke, and E. Beyer: Proc. SPIE 2014, (2014) 48.
[41] Y. Kiang and R. Lang: Appl. Opt., 22, (1983) 12196.
[42] J. Bonse, S. Höhm, S. Kirner, A. Rosenfeld, and J. Kruger: J Sel Top Quantum Electron, 23, (2017) 9000615.
[43] M. Bieda, M. Siebold, A. F. Lasagni: Appl. Surf. Sci., 387, (2016) 175.
[44] F. Bouchard, M. Soldera, R. Baumann, A. F. Lasagni: Materials, 14, (2021) 1756.

[45] B. Narijauskaitė, A. Palevicius, R. Gaidys, G. Janušas, and R. Šakalys: Sensors, 13, (2013) 11229.
[46] R. Česnavičius, S. Kilikevičius, P. Krasauskas, R. Dundulis, and H. Olišauskas: Mechanics, 22, (2016) 291.
[47] W. Piekarska, M. Kubiak, and Z. Saternus: Arch. Metall. Mater., 58, (2013) 1391.
[48] B. Käack and C. Malmberg: "Aluminium foil at multiple length scales, mechanical tests and numerical simulations in Abaqus" (Lund University, 2015) http://lup.lub.lu.se/student-papers/record/7451137.

(Received: June 3, 2022, Accepted: August 28, 2022)